Automatic Classification of Spirulina Microscopic Observations using Deep Learning Techniques

Tomoatsu Maguchi[1], Ulises Orozco-Rosas[1*], Kenia Picos[1]

[1]CETYS Universidad, Av. CETYS Universidad, No. 4, Fracc. El Lago, Tijuana, 22210, B.C., Mexico.

*Corresponding author(s). E-mail(s): ulises.orozco@cetys.mx;
Contributing authors: tmaguchi@cetys.edu.mx; kenia.picos@cetys.mx;

Abstract

The morphological condition of the microalgae organism *Arthrospira platensis* (commonly known as spirulina) in mass cultivation and industrial-scale operations is strongly influenced by environmental and operational factors. Changes in morphology can affect operational and quality parameters in both upstream and downstream processes. This work presents a deep learning architecture for the automatic classification of microscopic observations of *Arthrospira platensis*, framing the task as an automated model that analyzes microscopic images and supports human-centered decision-making informed by data-driven insights. Using a labeled dataset to train a convolutional neural network (CNN), the objective is to detect different microalgae conditions, including fragmentation, stress, and health. The model is intended to generate a numerical score for the image data based on patterns learned from features of different conditions. By enhancing operational decision-making through a human-centered approach, this work highlights the importance of Industry 5.0 in agriculture and biochemical processes, potentially shaping the field toward more data-driven insights. The evaluation of the experimental implementation presents high accuracy in terms of quantitative metrics.

Keywords: convolutional neural networks, image classification, Spirulina, Arthrospira platensis, microalgae monitoring, deep learning, industry 5.0

1 Introduction

Microalgae cultivation has gained considerable attention due to its nutritional value and sustainable biomass productivity, while requiring less resources compared to other higher plants. Microalgae cultivation requires only 0.5 to 1 m^2 of land and 240 to 2300 L of freshwater per kilogram of protein produced [1]. The use of microalgae has broad reaches, from nutraceuticals, food, pharmaceuticals, to bioremediation, and even extraction of essential compounds for diverse applications, such as phycocyanin for natural food colorant [2], and ergothioneine as bioactive compounds with antioxidant properties that may contribute to protection against oxidative stress [3]. Of all photosynthetic microorganisms, microalgae have had extremely high diversity with an estimated range of around 200,000 to 800,000 species, with only a fraction of about 50,000 to have been formally described [4, 5], and only a handful of which have been commercialized.

Among those in commercial use, *Arthrospira platensis*, which is a spiral morphological multicellular trichome filament, is one of the most well known in industrialized cultivation [6]. However, the task of observing the microscopic image of the organism in growth is still critical in maintaining and controlling the mass scale cultivation.

Microscopic image analysis for microalgae is similar to the task of a medical diagonosis, in which an expert is required to perform the classification and critical determination in this field of medical study for decision making. Similarly, observation of a microscopic image requires a seasoned culture control analyst to conduct the evaluation and determination of the condition [7].

However, this task not only requires time, but also has a significant dependency on the person conducting the observation. Additionally, traditional microscopic image analysis has lacked quantitative assessment of the observed condition, such as the degree of fragmentation of the algal organism at a given time, due to subjective recognition of the condition, rather than a standardized interpretation based on deep learning techniques. Automating the observation and classification of this task can address variability and inconsistencies, as well as reduce dependence on human expertise. Thus, creating a process of rapid, precise, and consistent analysis with quantitative determination by the computer (i.e., an accurate numerical score is highly required for this process).

In this work, we propose a deep learning approach through the application of a deep convolutional neural network framework model to identify morphological conditions of the microalgae, more specifically the level of culture damage represented by the amount of fragmented cells within a sample. The strategic approach is to establish a quantifiable value in the interpretation of the physiological condition of the microorganism in relation to its overall health and performance, which can be affected by the amount of hormogonia formation as a result of the fragmentation of the trichome in the necridia [6]. The objective is to evaluate the automation of the microscopic observation process to ameliorate the burden of the microscopic analysis task of the culture media.

Therefore, in this work, the CNN based framework for automatic microscopic image classification of *Arthrospira platensis* is proposed as a powerful tool to materialize the solution to the problem identified with traditional methodology that relied heavily

Table 1 AI and ML approaches for microalgae classification

AI/ML Algorithm	Application	Strain	Performance
RF [9]	Classification	*Chlorella vulgaris*	94.50% AUC
CNN [10]	Classification	*Acutodesmus obliquus*, *Monoraphidium sp.*, *Spirulina sp.*, *Tetradesmus deserticola*, *Desmodesmus perforatus*	89.00% accuracy
ANN [11]	Classification	*Chlorella*, *Scenedesmus*, *Haematococcus*, *Synechococcus*, *Chlamydopodium*, *Docystidium*	97.27% accuracy
CNN–SVM [12]	Classification	Cyanobacteria and Chlorophyta	99.66% accuracy
k-NN [13]	Classification	*Chlorella vulgaris* FSP-E, *Chlamydomonas reinhardtii*, *Spirulina platensis*	96.93% accuracy

Note. Adapted from "Artificial intelligence and/or machine learning algorithms in microalgae bioprocesses," by E. Imamoglu, 2024, *Bioengineering*, vol. 11, no. 11, Art. no. 1143 [8]. Individual studies are cited in the corresponding algorithm entries.

on the subjective interpretation of the culture condition. The objective is to support culture monitoring through automated feature learning and classification of morphological conditions associated with fragmentation and stress to assist the human in culture monitoring work.

The work is organized as follows. Section 2 presents the literature review and theoretical background related to artificial intelligence, machine learning, and deep learning approaches for microalgae classification. Section 3 describes the proposed CNN-based framework for the automatic classification of microscopic observations of *Arthrospira platensis*, including image acquisition and preprocessing, transfer learning, model training, and the inference approach for pond-level monitoring. Section 4 presents the experimental implementation and performance analysis, including the training and validation results, confusion matrix analysis, and quantitative inference results. Finally, Section 5 presents the conclusions and future work in AI-assisted monitoring of industrial spirulina cultivation.

2 Literature Review and Background Studies

The use of artificial intelligence (AI) and machine learning (ML) applications on biological images for analysis and interpretation of its morphological condition has been expanding during recent years due to advancements that have been made in the computational power and development in deep learning algorithms. Many studies have been conducted achieving high accuracies exceeding 90%, demonstrating that convolutional neural networks (CNNs) can be highly effective for feature learning. Table 1 presents AI and ML approaches for microalgae classification, adapted from Artificial intelligence and/or machine learning algorithms in microalgae bio-processes by E. Imamoglu (2024) [8]. In contrast, traditional microalgae classification methods, which are highly based on microscopic observations and morphological evaluation by human experts, are labor-intensive, time-consuming and dependent on skilled taxonomists [8].

A broad overview of artificial intelligence and machine learning approaches applied to microalgae classification is presented in Table **??**, where the Convolutional Neural Network (CNN) is listed along with traditional methods such as Random Forest (RF), Support Vector Machines (SVM), k-Nearest Neighbors (k-NN), and Artificial Neural Networks (ANN), which have also been used in different areas to classify microalgae. Although these methods have demonstrated high accuracy in classification applications in various microalgae species, they typically rely on manual features that are extracted from microscopic observations. The dependency on predefined features results in a limitation to fully capture the complex nature of the spatial and morphological characteristics found in microscopic image data.

However, Convolutional Neural Networks (CNNs) are far more suitable for image-based analysis because they can automatically and directly learn hierarchical spatial feature representations from raw images. Due to these capabilities, CNN-based approaches have been widely implemented in medical imaging, object recognition, and microscopic image classification tasks. CNNs are particularly effective for tasks that involve subtle variations in morphological aspects in the image, such as fragmentation of the cell structure filament and stress conditions in *Arthrospira platensis*. In this context, and building on top of this path from traditional machine learning to deep learning, Table 2 focuses on CNN-based approaches and its related deep learning architectures that have been applied to microscopic image classification.

Table 2 Primary deep learning approaches for microscopic image classification of microalgae

Method	**Task**	**Organism**	**Performance**	**Ref.**
CNN + Second-order Features	Image classification	Plankton (mixed species)	75.82%	[14]
CNN vs Vision Transformer	Image classification	Plankton	>90%	[15]
CNN	Automated classification	Marine microorganisms	93.7%	[16]
CNN + Grad-CAM	Image classification + interpretability	Microalgae	96.7%	[17]
AI-driven CNN models	Detection & classification	Toxic microalgae	93%	[18]

Note. Reported performance values correspond to different datasets and experimental setups, and therefore should not be interpreted as directly comparable. The table is intended to provide a general overview of deep learning approaches for microscopic image classification rather than a standardized benchmark.

Recent studies have demonstrated the applicability of convolutional neural networks (CNNs) for plankton and microorganism classification tasks. CNN architectures have been applied for plankton image classification using second-order feature extraction, while comparative studies between CNNs and Vision Transformers have also been reported for plankton recognition applications [14, 15]. Deep convolutional frameworks such as ZooplanktoNet have further demonstrated the feasibility of CNN-based approaches for zooplankton classification and aquatic microorganism analysis [16]. In addition, Grad-CAM interpretability methods have been incorporated into CNN-based microscopic algae classification systems to visualize image regions contributing to classification decisions [17].

Convolutional Neural Networks (CNNs) are feed-forward artificial neural network models inspired by the biological organization of the visual cortex [19]. A CNN architecture is typically composed of convolutional layers, nonlinear activation functions, pooling layers, and fully connected layers [19, 20]. These architectures are capable of automatically learning hierarchical spatial features directly from raw image data, making them particularly suitable for image classification applications.

During the training process, backpropagation is employed to compute the gradient of the loss function with respect to the network parameters. The optimization process iteratively updates the network parameters to minimize the loss function.

The forward propagation of a convolutional layer is mathematically represented by Eq. 1, which is dependent on a nonlinear activation operation σ [21].

$$x_j^{(l)} = \sigma\left(\sum_{i=1}^{N^{(l-1)}} x_i^{(l-1)} * w_{i,j}^{(l)} + b_j^{(l)}\right) \tag{1}$$

where $x_j^{(l)}$ represents the output feature map, $x_i^{(l-1)}$ denotes the input feature map from the previous layer, $w_{i,j}^{(l)}$ corresponds to the convolution kernel weights, $b_j^{(l)}$ represents the bias term, and σ denotes the nonlinear activation function.

The Rectified Linear Unit (ReLU) activation function commonly employed in CNN architectures is expressed as

$$ReLU(x) = \max(0, x) \tag{2}$$

In neural networks, categorical cross-entropy loss is commonly employed for multi-class classification problems because it measures the difference between the predicted probability distribution and the true class distribution. Lower loss values indicate that the predicted class probabilities are closer to the actual labels. The categorical cross-entropy loss function is expressed as follows:

$$\mathcal{L} = -\frac{1}{N}\sum_{i=1}^{N}\sum_{c=1}^{C} y_{i,c}\log(p_{i,c}) \tag{3}$$

where N represents the total number of samples, C corresponds to the total number of classes, $y_{i,c}$ is a binary indicator equal to 1 if class c is the correct classification for observation i, and $p_{i,c}$ denotes the predicted probability for class c corresponding to observation i. [22].

In a Convolutional Neural Network (CNN), the theoretical framework revolves around convolutional layers, activation functions, pooling layers, and fully connected layers as illustrated in Fig. 1. Convolutional layers apply filters to input data, capturing spatial features. Activation functions introduce non-linearity. Pooling layers reduce spatial dimensions while preserving essential information. Fully connected layers combine extracted features for classification [23].

The network is trained using backpropagation and optimization algorithms to minimize a defined loss function, adjusting weights for accurate predictions. This architecture enables CNNs to excel in tasks like image recognition as shown in the Fig. 2 [24].

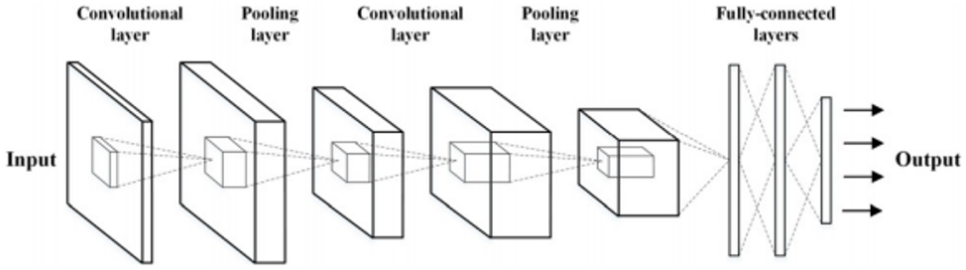

Fig. 1 Example of a convolutional neural network (CNN) pipeline illustrating convolution, ReLU activation, pooling, fully connected layers, and final image classification output.

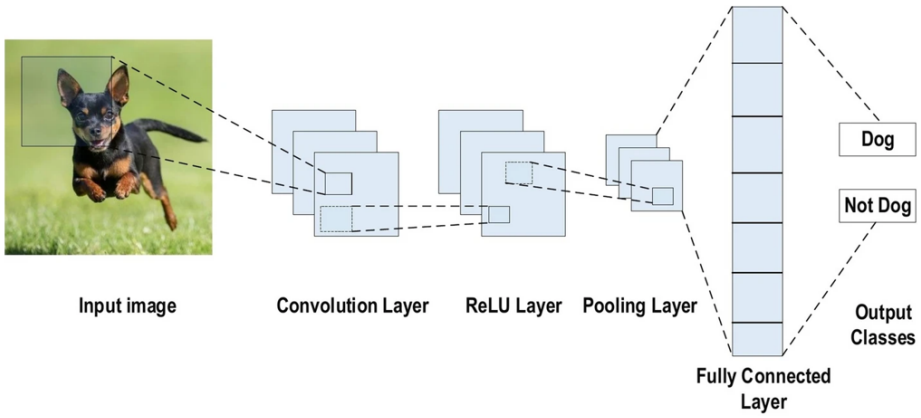

Fig. 2 Typical convolutional neural network architecture composed of convolutional layers, pooling layers, and fully connected layers

The last decade has witnessed revolutionary advances in deep learning, which has emerged as one of the most important developments in machine learning and artificial intelligence. Modern deep learning architectures have continuously outperformed conventional state-of-the-art techniques in computer vision and natural language processing applications [20, 25].

3 Proposed Scheme

A convolutional neural network framework is proposed for the automatic classification of microscopic observations of *Arthrospira platensis* cultivated under industrial-scale conditions (See Fig. 3). The proposed framework is intended to support

human-centered decision-making by assisting culture monitoring through automated microscopic image classification and morphological interpretation.

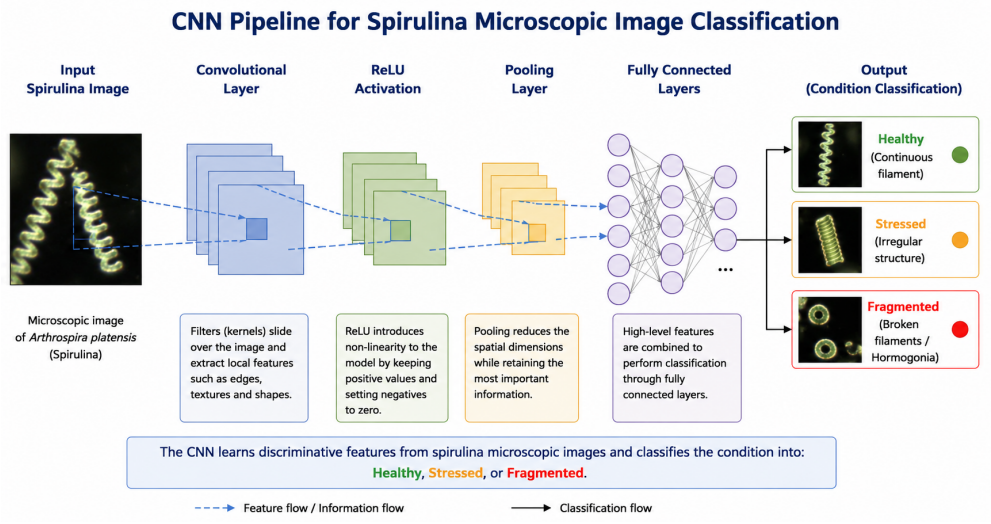

Fig. 3 Proposed convolutional neural network (CNN) pipeline for automatic classification of microscopic observations of *Arthrospira platensis*. The framework receives microscopic spirulina images as input and performs hierarchical feature extraction through convolutional, ReLU activation, and pooling layers. The extracted high-level features are subsequently processed through fully connected layers for multiclass classification into healthy, stressed, and fragmented conditions.

The proposed methodology consists of microscopic image acquisition, image preprocessing, CNN-based feature extraction, multiclass classification, and prediction analysis. The overall framework was inspired by real industrial production conditions from operational raceway ponds dedicated to spirulina cultivation at a biochemical plant in Imperial Valley, California.

3.1 Inference and Pond-Level Monitoring

After model training, an inference pipeline was implemented to apply the trained CNN model to new microscopic images not used during training. The inference procedure loads the best saved checkpoint and applies the same validation transformation used during model evaluation, including resizing, tensor conversion, and normalization.

To evaluate complete microscopic images, each input image is divided into multiple sub-images before classification. In this work, the complete image is divided into a 10×10 grid, generating 100 sub-images. Each sub-image is classified by the trained CNN model, and the predicted class counts are accumulated to estimate the distribution of morphological conditions within the full microscopic observation.

The inference process generates class-level statistics for each image, including the number of fragmented, tight, relaxed, and empty regions detected. These outputs are

stored as tabular data for further analysis and can be exported into CSV files for seasonal or pond-level monitoring.

The complete inference workflow can be summarized as follows:

$$I_{full} \rightarrow \{I_1, I_2, \ldots, I_{100}\} \rightarrow CNN(I_k) \rightarrow \{C_f, C_t, C_r, C_e\} \tag{4}$$

where I_{full} represents the complete microscopic image, I_k denotes each sub-image, with $k \in \{1, 2, \ldots, 100\}$, C_f, C_t, C_r, and C_e corresponding to the accumulated counts for fragmented, tight, relaxed, and empty regions, respectively.

This strategy allows the model to move beyond single-image classification and toward quantitative image-level monitoring, where the proportion of each morphological condition can be used as an indicator of culture status.

3.2 Microscopic Image Acquisition

The microscopic image dataset is obtained from cultivation samples collected daily from industrial production raceway ponds. Microscopic observations are captured using a digital microscope system under controlled illumination and magnification conditions to reduce acquisition variability.

The collected dataset contains images corresponding to different physiological and morphological conditions of *Arthrospira platensis*, including fragmented (see Fig. 4), stressed (see Fig. 5) and healthy (see Fig. 6). Healthy cultures generally exhibit continuous spiral filament structures, while stressed or fragmented samples present trichome breakage, irregular morphology, and increased hormogonia formation.

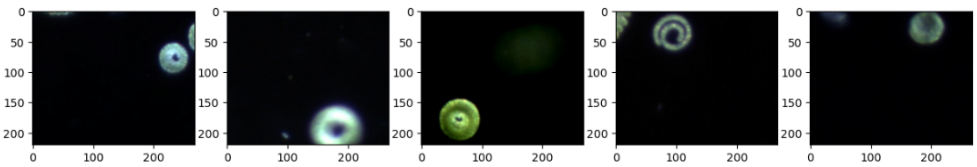

Fig. 4 Class: 1-fragmented. Examples of fragmented *Arthrospira platensis* microscopic observations employed during CNN training. Fragmented spirulina conditions are characterized by broken filaments, hormogonia formation, incomplete trichome structures, and reduced filament continuity, which are commonly associated with physiological stress and culture deterioration.

The proposed framework envisions the future integration of robotic-assisted sample handling systems and automated microscopic acquisition platforms to further reduce human dependency during microscopic observation and sample manipulation. The Fig. 7 illustrates a six-axis robotic arm equipped with a pipette as the end-effector for automated sample manipulation for analytical procedures undertaken in the culture laboratory.

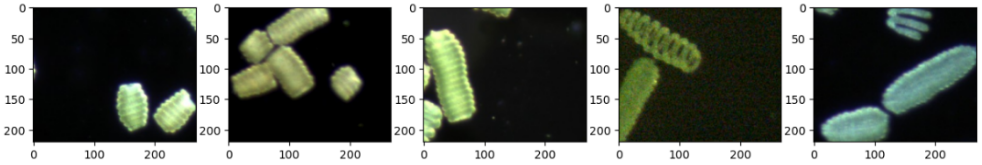

Fig. 5 Class: 2-tight. Examples of stressed *Arthrospira platensis* microscopic observations employed during CNN training. Stressed spirulina conditions exhibit tightly coiled filaments, abnormal morphology, irregular trichome structures, and morphological deformation associated with environmental or operational stress conditions.

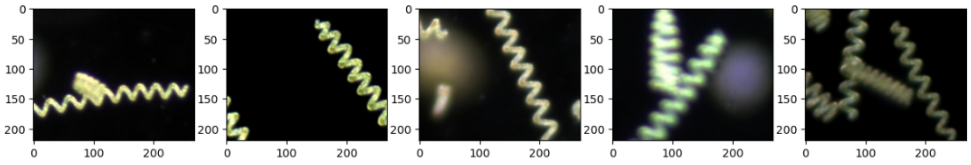

Fig. 6 Class: 3-relaxed. Examples of healthy *Arthrospira platensis* microscopic observations employed during CNN training. Healthy spirulina conditions are characterized by continuous spiral filament structures, uniform morphology, and intact trichomes indicative of stable physiological growth conditions.

3.3 Image Preprocessing and Dataset Generation

Image preprocessing is employed to improve feature consistency and prepare the dataset for CNN training. The preprocessing stage includes image normalization, resizing, and automatic generation of sub-images through a Python-based image processing algorithm.

The preprocessing algorithm divides each original microscopic image into 100 smaller sub-images through horizontal and vertical segmentation operations. The resulting sub-images are automatically stored into dedicated database folders according to their corresponding class labels.

Data augmentation techniques including image rotation, reflection, scaling, and brightness variation are additionally applied to improve model generalization capability and reduce overfitting during training.

The organized datasets are subsequently divided into training, validation, and testing subsets to support supervised learning and model evaluation.

3.4 CNN Architecture and Transfer Learning

The proposed classification model was implemented using the PyTorch deep learning framework. A transfer learning strategy was adopted using a pretrained ResNet50 architecture. The final fully connected layer of ResNet50 was modified to match the number of microscopic image classes in the dataset.

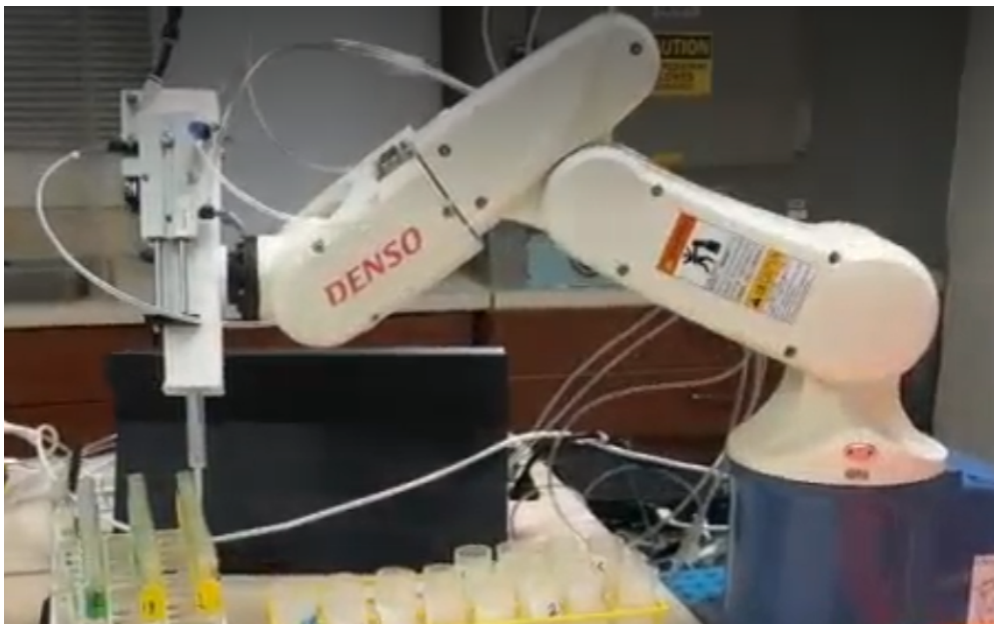

Fig. 7 Example of a robotic-assisted laboratory platform for automated liquid handling and sample manipulation. Robotic systems may support future automated microscopic sample preparation and image acquisition workflows for *Arthrospira platensis* monitoring applications, reducing manual handling variability and improving operational consistency.

The model receives RGB microscopic images as input and internally resizes the input tensor to 224×224 pixels before feature extraction. ResNet50 was selected because residual connections allow deeper convolutional architectures to be trained more effectively by reducing degradation problems associated with very deep networks.

The classification layer was replaced as follows:

$$f_{out} = Wh + b \tag{5}$$

where h represents the feature vector extracted by the pretrained ResNet50 backbone, W denotes the trainable weights of the final classification layer, and b is the bias term. The output dimension corresponds to the number of classes used for spirulina condition classification.

The model was trained using the cross-entropy loss function and the Adaptive Moment Estimation (Adam) optimizer with a learning rate of 1×10^{-4}.

3.5 Training Procedure and Optimization

The CNN model is trained using supervised learning with labeled microscopic image data. During training, backpropagation is employed to compute the gradients of the loss function with respect to the trainable network parameters.

Categorical cross-entropy loss, as defined in the Eq. (3), is employed for multiclass classification because it measures the difference between the predicted probability distribution and the true class distribution.

The Adam optimization algorithm is employed during training to iteratively update the network parameters and minimize the loss function.

The proposed framework is intended to support early detection of abnormal culture conditions before progressive deterioration impacts operational productivity and product quality.

4 Experiments and Performance Analysis

This section presents the experimental implementation and performance evaluation of the proposed CNN-based framework for the classification of microscopic observations of *Arthrospira platensis*. The experimental setup and model configuration are first described, followed by an analysis of the training and validation performance. Finally, the classification and inference results are examined to assess the capability of the proposed approach to identify and quantify morphological conditions in microscopic images.

4.1 Experimental Environment

The experimental implementation was conducted using Python (3.12.4) and the PyTorch (2.3.0) deep learning framework. The model was trained using Graphics Processing Unit (GPU) Quadro RTX3000 acceleration through Computer Unified Device Architecture (CUDA 12.1). In the absence of a GPU in the environment, the processing took place with the Central Processing Unit (CPU). The training pipeline included image preprocessing, data augmentation, class balancing, model training, validation, checkpoint saving, and confusion matrix analysis.

The microscopic image dataset was organized using the "Image Folder" structure, where each folder represented a class label. The dataset was balanced by identifying the class with the minimum number of samples and randomly selecting the same number of images from each class. This approach was used to reduce class imbalance during training.

The dataset was divided into 80% training data and 20% validation data. Training images were resized to 220×268 pixels and augmented using horizontal flipping and color jittering. Validation images were resized and normalized without random augmentation. Table 3 shows the experimental parameters used during CNN training.

In order to ensure stability in the inference, the model was set to evaluation mode by using model.eval(). This is to disable operations which are specific to training, such as dropout and batch normalization updates from interfering with the deterministic behavior during prediction.

The inference images were processed using the same normalization parameters applied during validation. Each image was converted to RGB format, resized to the selected image dimensions, converted to a tensor, and normalized using ImageNet mean and standard deviation values.

Table 3 Experimental parameters used during CNN training

Parameter	**Value**
Framework	PyTorch
Model Architecture	ResNet50 Transfer Learning
Input Image Size	220×268 pixels
Internal ResNet Input Size	224×224 pixels
Batch Size	32
Epochs	20
Optimizer	Adam
Learning Rate	1×10^{-4}
Loss Function	Cross-Entropy Loss
Scheduler	ReduceLROnPlateau
Training/Validation Split	80% / 20%
Acceleration	CUDA GPU when available

The inference pipeline was designed to scan individual images, folders of images, and complete pond-level image directories. Date information was extracted from image filenames when available, allowing prediction statistics to be organized across time for seasonal monitoring.

4.1.1 Preprocessing and Data Augmentation

The preprocessing pipeline consisting of image resizing, tensor conversion and normalization, involved image resizing to ensure consistent input dimensions enabling stable tensor generation and batch processing during CNN training. The images were normalized using the ImageNet mean and standard deviation values, which is appropriate for transfer learning with pretrained ResNet architectures. Augmentations techniques, such as random horizontal flipping and color jittering with brightness and contrast variation were applied to improve model robustness against image orientation differences and illumination variability observed in microscopic image acquisition.

The training transformation is summarized as follows:

$$T_{\text{train}} = \{\text{Resize}, \text{Flip}, \text{ColorJitter}, \text{Tensor}, \text{Normalize}\} \tag{6}$$

where T_{train} represents the transformation pipeline applied to the training dataset.

4.1.2 Training and Validation Procedure

The model was trained with a batch size of 32 for 20 epochs using mini-batch gradient optimization, while cross-entropy loss was calculated and the model parameters were being updated through backpropagation.

During the training, the model checkpoint corresponding to the highest validation accuracy was saved. The epoch number, training losses, validation losses, training accuracies as well as validation accuracies were stored at each checkpoint.

4.2 Results and Discussion

The training process generated loss and accuracy curves for both the training and validation subsets, the which were used to evaluate learning effectiveness, performance

on unseen data, and whether overfitting condition were to be observed. The validation loss was also monitored to adjust the learning rate.

The classification performance of the model was evaluated using a confusion matrix and a classification report. The confusion matrix visualizes the distribution of the correct and incorrect predictions across the different spirulina morphological condition by classes.

Accuracy was calculated [26] as

$$Accuracy = \frac{TP + TN}{TP + TN + FP + FN} \tag{7}$$

where TP and TN represent true positive and true negative predictions, while FP and FN represent false positive and false negative predictions.

Precision, recall, and F1-score were calculated [26] as

$$Precision = \frac{TP}{TP + FP} \tag{8}$$

$$Recall = \frac{TP}{TP + FN} \tag{9}$$

$$F1 = 2 \cdot \frac{Precision \cdot Recall}{Precision + Recall} \tag{10}$$

It was possible to take advantage of pretrained image feature extraction with the use of ResNet50 transfer learning on the model. This approach is especially useful when the available dataset is relatively small, because the pretrained model already contains visual feature knowledge learned from large image datasets. However, microscopic spirulina images present specific challenges that differ from conventional image classification datasets. These include illumination variation, focus differences, partial filaments, overlapping organisms, and similar morphology between stressed and healthy conditions. Therefore, confusion matrix analysis is essential to identify whether the model is confusing specific classes, particularly tightly coiled stressed samples and relaxed healthy filaments.

The training bias was reduced by incorporating class balancing technique, the which is done by reducing the number of samples in larger classes to match the class with the fewest images. Although this technique helped reduce bias on classes containing larger number of training samples, it also resulted in a decrease in the total number of images available for training. Future work may evaluate alternative balancing strategies, including weighted cross-entropy loss, oversampling, and class-aware data augmentation.

The training and validation performance of the proposed ResNet50 transfer learning framework was evaluated through loss and accuracy monitoring across training epochs. These metrics were applied to evaluate the behavior for convergence, stability, as well as in the capability for model generalization.

The training and validation curves obtained during CNN optimization are shown in the Figure 8. The training loss can be observed to decreased along the training process, and the training accuracy shows an improving trend, which is an indication that the feature learning and parameter optimization were both successfully achieved by the model.

Fig. 8 Training and validation loss and accuracy curves obtained during CNN training using the ResNet50 transfer learning architecture. The loss curves illustrate the optimization behavior of the model, while the accuracy curves demonstrate the classification performance evolution across training epochs. The observed fluctuations in validation accuracy suggest the presence of dataset variability and limited generalization caused by the relatively small microscopic image dataset.

On the other hand, the validation curves exhibited greater variability compared to the training curves, suggesting the presence of dataset variability and limited generalization capability associated with the relatively small microscopic image dataset. The validation accuracy, however, remained above 80% during the later training epochs, indicating that the proposed CNN framework has the capability to classify different spirulina morphological conditions. The best validation accuracy achieved by the ResNet50 transfer learning framework was 84.7%, the which in terms of macro F1-score is 0.83.

Potential presence of overfitting can be detected in certain epochs, the which is evidenced in the divergence that can be observed between training and validation performance, suggesting the potential presence of overfitting. This behavior confirms the importance of future dataset expansion, additional data augmentation strategies, and regularization approaches to further improve model robustness and generalization performance.

To further evaluate the classification capability of the proposed CNN framework, a confusion matrix was generated using the validation dataset. The confusion matrix provides a detailed distribution of the prediction behavior across all spirulina condition classes.

Figure 9 illustrates the confusion matrix generated during validation. A good representation of the spirulina morphological conditions by the model can be observed in this matrix as most predictions are in alignment with the diagonal line of the matrix.

The fragmented and tight classes demonstrated particularly strong classification performance, as most samples were observed to be correctly identified by the model.

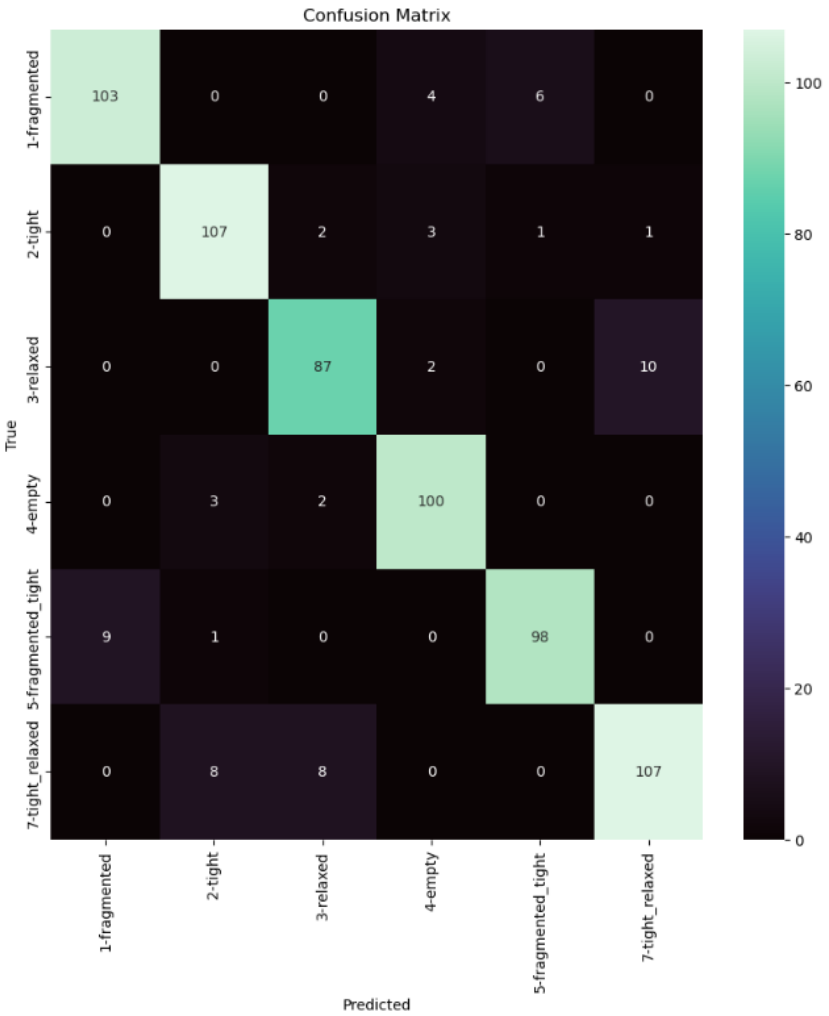

Fig. 9 Confusion matrix obtained from the CNN classification results for microscopic observations of *Arthrospira platensis*. The matrix illustrates the distribution of correct and incorrect predictions across fragmented, tight, relaxed, empty, fragmented-tight, and tight-relaxed classes. Higher values along the diagonal indicate strong classification performance for the corresponding classes.

However, several misclassifications were observed between relaxed and tight relaxed conditions, the which is suggesting morphological similarities between these classes.

The observed confusion between related filament structures is expected because spirulina morphology may present gradual transitions between physiological states rather than perfectly discrete conditions. Despite these challenges, the confusion matrix demonstrates that the proposed CNN framework successfully learned discriminative features associated with multiple spirulina morphological patterns.

The inference pipeline expands the model application from individual classification to image-level and pond-level monitoring. By dividing complete microscopic images

into 100 sub-images, the system generates quantitative counts of the detected morphological classes. This approach provides a more informative interpretation than a single image label because it estimates the relative presence of fragmented, tight, relaxed, and empty regions within the full observation. A summary of the generated outputs is presented in Table 4.

Table 4 Summary of inference pipeline outputs

Output	**Description**
Predicted class	Classification assigned to each sub-image
Class counts	Number of sub-images classified as fragmented, tight, relaxed, or empty
Sample predictions	Representative predicted sub-images stored for reporting
CSV output	Tabular file containing prediction statistics for further analysis
Seasonal trend	Time-series plot of fragmentation counts by pond and date

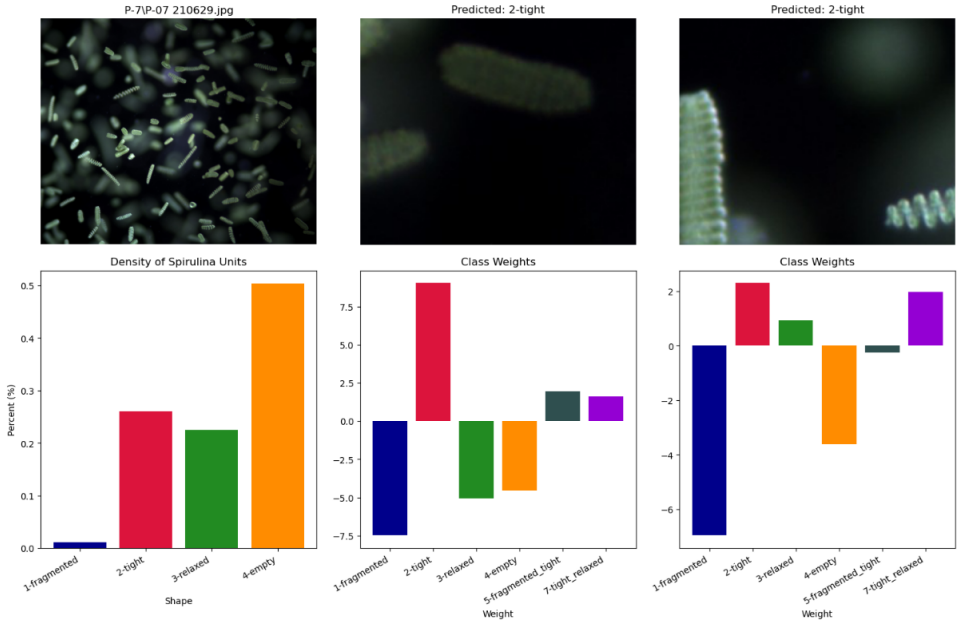

Fig. 10 Example of the CNN inference and prediction analysis pipeline applied to a microscopic observation of *Arthrospira platensis*. The upper panels illustrate the original microscopic image together with representative sub-images classified by the CNN model. The lower panels present the estimated density distribution and class-weight analysis generated during inference. The results demonstrate the capability of the proposed framework to quantify the relative distribution of fragmented, tight, relaxed, and empty regions within complete microscopic observations.

Figure 10 illustrates a representative prediction report generated by the inference pipeline. The system divides the complete microscopic observation into multiple

sub-images and evaluates each region independently using the trained CNN model. The resulting class predictions are aggregated to estimate the relative distribution of spirulina morphological conditions within the complete image.

The prediction report additionally provides density estimation and class-weight visualization, allowing rapid interpretation of dominant morphological conditions. This type of quantitative analysis may support operational monitoring by identifying increasing fragmentation trends or abnormal morphological patterns associated with culture stress.

The generated CSV outputs allow prediction results to be tracked over time for individual production ponds. In this way, the fragmentation count can be plotted as a temporal indicator of culture condition during a production season. This provides a potential pathway for converting microscopic observations into operational monitoring signals.

The inference process is particularly relevant for industrial implementation because complete microscopic images may contain multiple organisms or regions with different morphological conditions. Sub-image scanning allows the model to evaluate localized image regions and aggregate the results into a quantitative summary. This supports the objective of reducing subjective interpretation and improving consistency in culture monitoring.

5 Conclusions

This work presented a deep learning framework for the automatic classification of microscopic observations of *Arthrospira platensis*. The proposed implementation used a PyTorch-based ResNet50 transfer learning model to classify spirulina microscopic images according to morphological condition.

The experimental approach included image preprocessing, data augmentation, class balancing, transfer learning, mixed precision training, validation monitoring, checkpoint saving, and confusion matrix evaluation. The use of ResNet50 provided a practical strategy for improving feature extraction when the available microscopic image dataset is limited.

The proposed framework demonstrates the potential of CNN-based image classification to support industrial spirulina culture monitoring by reducing dependency on subjective visual interpretation. Rather than replacing expert analysis, the model is intended to support human-centered decision-making by providing rapid and standardized microscopic classification.

In addition to model training and validation, the developed inference pipeline enables complete microscopic images to be divided into sub-images and analyzed quantitatively. This allows class counts to be extracted from each observation and organized over time for pond-level monitoring. Therefore, the proposed framework provides a foundation not only for image classification, but also for future development of operational indicators related to spirulina culture condition.

Acknowledgements. The authors would like to acknowledge Jacobo Puga for his valuable contributions to the experimental and development activities conducted at the biochemical plant during his participation in the summer internship program.

His support in data collection, preliminary testing, and research-related activities contributed to the development of this work.

References

[1] Wong, N., Ting, M., Kim, J.: Exploring microalgae protein: Quantity, quality and sustainability compared to conventional sources. Trends in Food Science & Technology **163**, 105188 (2025) https://doi.org/10.1016/j.tifs.2025.105188

[2] Lin, J., Pang, Y., Huo, Y., Jiang, J., Zhou, B., Shang, C.: Extraction, purification and characterization of spirulina phycocyanin. Algal Research **85**, 103861 (2025) https://doi.org/10.1016/j.algal.2024.103861

[3] Cordell, G.A., Lamahewage, S.N.S.: Ergothioneine, ovothiol a, and selenoneine—histidine-derived, biologically significant, trace global alkaloids. Molecules **27**(9), 2673 (2022) https://doi.org/10.3390/molecules27092673

[4] Hachicha, R., Elleuch, F., Ben Hlima, H., Dubessay, P., Baynast, H., Delattre, C., Pierre, G., Hachicha, R., Abdelkafi, S., Michaud, P., Fendri, I.: Biomolecules from microalgae and cyanobacteria: Applications and market survey. Applied Sciences **12**(4), 1924 (2022) https://doi.org/10.3390/app12041924

[5] Pierre, G., Delattre, C., Dubessay, P., Jubeau, S., Vialleix, C., Cadoret, J.-P., Probert, I., Michaud, P.: What is in store for eps microalgae in the next decade? Molecules **24**(23), 4296 (2019) https://doi.org/10.3390/molecules24234296

[6] Jung, C.H.G., Braune, S., Waldeck, P., Küpper, J.-H., Petrick, I., Jung, F.: Morphology and growth of arthrospira platensis during cultivation in a flat-type bioreactor. Life **11**(6), 536 (2021) https://doi.org/10.3390/life11060536

[7] Kaewman, N., *et al.*: A deep learning approach for locating microalgae in images captured by smartphone and digital microscope camera. In: 2023 Joint International Conference on Digital Arts, Media and Technology with ECTI Northern Section Conference on Electrical, Electronics, Computer and Telecommunications Engineering (ECTI DAMT & NCON), pp. 457–462. IEEE, Phuket, Thailand (2023). https://doi.org/10.1109/ECTIDAMTNCON57770.2023.10139572

[8] Imamoglu, E.: Artificial intelligence and/or machine learning algorithms in microalgae bioprocesses. Bioengineering **11**(11), 1143 (2024) https://doi.org/10.3390/bioengineering11111143

[9] Reimann, R., Zeng, B., Jakopec, M., Burdukiewicz, M., Petrick, I., Schierack, P., Rödiger, S.: Classification of dead and living microalgae Chlorella vulgaris by bioimage informatics and machine learning. Algal Research **48**, 101908 (2020) https://doi.org/10.1016/j.algal.2020.101908

[10] Hisham, S.D., Mohamad, S.E., Shapiai, M.I., Iwamoto, K., Hussin, A.A., Abdullah, N., Akhir, F.N.M.: Comparison of conventional cnn sequential api and functional api for microalgae identification. Journal of Advanced Research in Micro and Nano Engineering **17**, 96–104 (2024)

[11] Otálora, P., Guzmán, J.L., Acién, F.G., Berenguel, M., Reul, A.: An artificial intelligence approach for identification of microalgae cultures. New Biotechnology **77**, 58–67 (2023) https://doi.org/10.1016/j.nbt.2023.02.002

[12] Sonmez, M.E., Eczacıoglu, N., Gumuş, N.E., Aslan, M.F., Sabanci, K., Aşikkutlu, B.: Convolutional neural network–support vector machine based approach for classification of cyanobacteria and chlorophyta microalgae groups. Algal Research **61**, 102568 (2022) https://doi.org/10.1016/j.algal.2021.102568

[13] Chong, J.W.R., Khoo, K.S., Chew, K.W., Ting, H.Y., Iwamoto, K., Ruan, R., Ma, Z., Show, P.L.: Artificial intelligence-driven microalgae autotrophic batch cultivation: A comparative study of machine and deep learning-based image classification models. Algal Research **79**, 103400 (2024) https://doi.org/10.1016/j.algal.2024.103400

[14] Du, A., Gu, Z., Yu, Z., Zheng, H., Zheng, B.: Plankton image classification using deep convolutional neural networks with second-order features. In: Global Oceans 2020: Singapore – U.S. Gulf Coast, pp. 1–5 (2020). https://doi.org/10.1109/IEEECONF38699.2020.9389034

[15] Nanni, L., Lumini, A., Barcellona, L., Ghidoni, S.: Convolutional neural networks and vision transformers for plankton classification. Ecological Informatics **90**, 103272 (2025) https://doi.org/10.1016/j.ecoinf.2025.103272

[16] Dai, J., Wang, R., Zheng, H., Ji, G., Qiao, X.: Zooplanktonet: Deep convolutional network for zooplankton classification. In: OCEANS 2016 - Shanghai, pp. 1–6 (2016). https://doi.org/10.1109/OCEANSAP.2016.7485680

[17] Ali, M., Yaseen, M., Ali, S., Kim, H.-C.: Deep learning-based approach for microscopic algae classification with grad-cam interpretability. Electronics **14**(3), 442 (2025) https://doi.org/10.3390/electronics14030442

[18] Khemakhem, F., *et al.*: Ai-driven detection and classification of toxic microalgae. In: 2025 IEEE Afro-Mediterranean Conference on Artificial Intelligence (AMCAI), pp. 1–9 (2025). https://doi.org/10.1109/AMCAI66110.2025.11474367

[19] Correa, I., Drews, P., Botelho, S., Souza, M.S., Tavano, V.M.: Deep learning for microalgae classification. In: 2017 16th IEEE International Conference on Machine Learning and Applications (ICMLA), pp. 20–25. IEEE, Cancun, Mexico (2017). https://doi.org/10.1109/ICMLA.2017.0-183

[20] Krichen, M.: Convolutional neural networks: A survey. Computers **12**(8), 151

(2023) https://doi.org/10.3390/computers12080151

[21] Liu, L., Ouyang, W., Wang, X., *et al.*: Deep learning for generic object detection: A survey. International Journal of Computer Vision **128**, 261–318 (2020) https://doi.org/10.1007/s11263-019-01247-4

[22] Razali, M.N., Arbaiy, N., Lin, P.-C., Ismail, S.: Optimizing multiclass classification using convolutional neural networks with class weights and early stopping for imbalanced datasets. Electronics **14**(4), 705 (2025) https://doi.org/10.3390/electronics14040705

[23] Chai, Z.: Thermal radiation image based on neural network algorithm for muscle balance simulation during exercise training: Thermal conduction of exercise cells. Thermal Science and Engineering Progress **57**, 103139 (2025) https://doi.org/10.1016/j.tsep.2024.103139

[24] Shan, Q., Yang, Q., Ding, J., Hou, Y., Gu, K., Sun, Z., Zhou, J.: Comparison of different object detection and classification models. Highlights in Science, Engineering and Technology **34**, 218–224 (2023) https://doi.org/10.54097/hset.v34i.5559

[25] LeCun, Y., Bengio, Y., Hinton, G.: Deep learning. Nature **521**(7553), 436–444 (2015) https://doi.org/10.1038/nature14539

[26] Sujon, K.M., Hassan, R., Choi, K., *et al.*: Accuracy, precision, recall, F1-score, or MCC? Empirical evidence from advanced statistics, ML, and XAI for evaluating business predictive models. Journal of Big Data **12**, 268 (2025) https://doi.org/10.1186/s40537-025-01313-4